Physics of Fluids

The role of entrance functionalization in carbon nanotube-based nanofluidic systems: An intrinsic challenge

Cite as: Phys. Fluids **33**, 012015 (2021); https://doi.org/10.1063/5.0037208
Submitted: 13 November 2020 . Accepted: 31 December 2020 . Published Online: 27 January 2021

Ran Tao, Xiang Gao, Dewu Lin, Yixuan Chen, Yakang Jin, Xibing Chen, Shuhuai Yao, Pingbo Huang, Jin Zhang, and Zhigang Li

Physics of Fluids ARTICLE scitation.org/journal/phf

The role of entrance functionalization in carbon nanotube-based nanofluidic systems: An intrinsic challenge

Cite as: Phys. Fluids 33, 012015 (2021); doi: 10.1063/5.0037208
Submitted: 13 November 2020 • Accepted: 31 December 2020 •
Published Online: 27 January 2021

Ran Tao,[1] Xiang Gao,[1,2] Dewu Lin,[3] Yixuan Chen,[4] Yakang Jin,[1] Xibing Chen,[5] Shuhuai Yao,[1] Pingbo Huang,[4,5] Jin Zhang,[3,a)] and Zhigang Li[1,b)]

AFFILIATIONS

[1]Department of Mechanical and Aerospace Engineering, The Hong Kong University of Science and Technology, Clear Water Bay, Kowloon, Hong Kong
[2]Department of Physical Chemistry, School of Chemistry, The Sackler Center for Computational Molecular and Materials Science, Tel Aviv University, Tel Aviv 6997801, Israel
[3]Center for Nanochemistry, Beijing Science and Engineering Center for Nanocarbons, Beijing National Laboratory for Molecular Sciences, College of Chemistry and Molecular Engineering, Peking University, Beijing 100871, People's Republic of China
[4]Department of Chemical and Biological Engineering, The Hong Kong University of Science and Technology, Clear Water Bay, Kowloon, Hong Kong
[5]Division of Life Science, The Hong Kong University of Science and Technology, Clear Water Bay, Kowloon, Hong Kong

[a)]**E-mail:** jinzhang@pku.edu.cn
[b)]**Author to whom correspondence should be addressed:** mezli@ust.hk

ABSTRACT

In this work, experiments, molecular dynamics (MD) simulations, and theoretical analysis are conducted to study ion transport in thin carbon nanotubes (CNTs). Diverse nonlinear relationships between the ionic conductance (G) and the ion concentration (C) are observed. MD simulations show that the distinct G–C dependences are caused by the functionalization of the CNT entrance, which affects the energy barrier for ion transport and changes the ionic conductance. The various G–C relationships are also predicted using the electrokinetic theory by considering the potential generated by the functional groups at the CNT entrance. Practically, the number of functional groups at the CNT entrance is influenced by several factors, including both intrinsic and external effects, which make it difficult to regulate the ionic conductance and pose a challenge to CNT-based nanofluidic systems in practical applications.

I. INTRODUCTION

A fluidic system starts to accommodate new flow phenomena when its dimensions become comparable to or smaller than certain characteristic lengths, such as the Debye length and the typical molecular interaction distance.[1–4] A great number of new mechanisms that lead to diverse flow phenomena have been reported in nanoscale fluidic systems,[5–8] where fluid–wall molecular interactions play a critical role. Carbon nanotube (CNT) based fluidic systems are unique platforms for studying nanoscale fluid flows and molecular transport due to extraordinary physical properties of CNTs, such as nanoscale diameters, extremely smooth surface, and non-wetting properties. Fluid flows in CNTs have been extensively explored in the literature. In particular, ion transport in CNTs has attracted great attention due to the potential applications in broad areas, including flow sensing,[9] drug delivery,[10] energy conversion,[11,12] and seawater desalination.[13,14] In addition to the small sizes and hydrophobic surfaces, CNTs can also be made to bear high permeability and excellent selectivity for ion transport,[15–18] which are typically owned by certain biological ion channels. Therefore, if CNT-based ion transport devices can be easily made practical, they will have significant impacts on various areas.

TABLE I. *G–C* power-law relationships for ion transport in CNTs in the literature (the conductance was obtained at $C = 1$ M).

CNT length	CNT diameter	Conductance	α in $G \propto C^{\alpha}$	Reference
2 μm	1.8 nm	0.025 nS–26.75 nS	0.33–0.4	19
20 μm	1.7 nm	50 nS	0.37	23
20 μm	1.5 nm	70 nS–140 nS	0.5	22
1–3 μm	7 nm–70 nm	0.2 nS–40 nS	1/3	21
~10 nm	0.8 nm	69 pS	0.5 (pH = 7.5) 1 (pH = 3)	25
10 nm	1.5 nm	766 pS	2/3	24
5 nm–15 nm	1.51 nm	630 pS	1	28
40 μm	1.2 nm–2.0 nm	3 pS–49 pS	$\alpha < 1$	27
100 μm	1.6 nm	9 pS–330 pS	$0.36 \leq \alpha \leq 0.72$	This work

Unfortunately, the fabrication of CNT-based nanofluidic systems is nontrivial and there are several issues that cause the transport of ions unpredictable.[19–29] In the past two decades, extensive efforts have been devoted to studying ion transport in CNTs. Quite a few intriguing phenomena have been observed, such as fast ion transport (or high ionic conductance), stochastic currents, and ionic rectification. However, some of the previous findings are contradictory. For example, many experimental studies have found that the ionic conductance, G, for isolated CNTs follows a power-law dependence on the ion concentration C, i.e., $G \propto C^{\alpha}$, which is different from the linear relationship in bulk systems. Nonetheless, the values of the power α are inconsistent. Values ranging from 1/3 to 2/3 have been reported,[19–25] as summarized in Table I. Other than the power-law dependence, saturation behavior of G at high concentrations has also been observed in experiments.[22,25] Various reasons have been proposed to explain the distinct G–C relationships.[21,22,24,25,30] Although most of them sound reasonable for specific cases, what exactly determines the G–C relationship remains unclear.

Some studies on nanoscale transport phenomena indicate that the CNT size plays an essential role in ion transport.[31–33] In thick CNTs, surface charges are of great importance in affecting the dynamics of ions.[21] For thin CNTs, however, the entrance properties, such as entrance functional groups, are more critical than the surface charges.[34–36] Compared with the surface charges, the entrance functionalization for thin CNTs is less controllable because it is affected by intrinsic factors (e.g., CNT size) and external effects, such as the fluid/solution properties and the fabrication process. These factors bring about uncertainty to the ion transport in CNTs.

In this work, we study ion transport in small-diameter CNTs through experiments, molecular dynamics (MD) simulations, and theoretical analysis. We aim at probing the mechanisms governing the various G–C behaviors. In experiments, different nonlinear G–C relationships are observed. They are either power laws with the power ranging from 0.36 to 0.72 or a non-monotonic dependence, where G increases first and then decreases with the increase in the ion concentration. These distinct G–C relationships are determined by the entrance functionalization, as confirmed by MD simulations and theoretical analysis. The uncertainty associated with the functional groups suggests that ion transport in thin CNTs is unpredictable, which is an intrinsic challenge to the practical applications of CNT-based nanofluidic systems. We expect that the current work can attract further efforts to tackle the problem to promote the applications of CNT-based ion transport.

II. METHODS

A. Carbon nanotube synthesis

Long, single-walled CNTs (SWCNTs) were synthesized through the chemical vapor deposition (CVD) method[37,38] on a SiO_2/Si substrate ($6 \times 10\,mm^2$), which was a Si wafer covered with a 300-nm-thick oxide layer. After the cleaning, the substrate was predefined with alignment markers for tracking CNTs at a later step. A $FeCl_3$ ethanol solution (0.05 mM) was then applied onto the short edge of the substrate before the substrate was placed in a quartz tubular furnace with a diameter of 1 in. The substrate was heated up and maintained at 950 °C in the furnace for 5 min. After the furnace was purged with 300 sccm argon, an Ar/H_2 (300 sccm/100 sccm) gas mixture was introduced for 5 min to activate the Fe catalysts. This was followed by a flow of 100 sccm argon passing through an ethanol bubbler, which was used as the carbon source, for 30 min. During this period, long SWCNTs, initiated by the catalysts, grew in the flow direction, i.e., parallel to the substrate surface. The typical length of the CNTs in 30 min was several millimeters. Finally, the CVD system was cooled down to room temperature in the argon atmosphere.

B. Device fabrication

After the growth of CNTs on a SiO_2/Si substrate, long and straight CNTs were selected and, on the basis of the markers, their relative locations were acquired by using a scanning electron microscope (SEM, JEOL JSM-7100F). An SEM image of a long SWCNT is shown in Fig. 1(a). The substrate grown with CNTs was then coated by a layer of 800-nm-thick PMMA photoresist (MicroChem Co., 950 PMMA A5), and two reservoirs were patterned on it by a standard electron beam lithography (EBL) process [Fig. 1(b)]. This was followed by a treatment in the PMMA developer (methyl isobutyl ketone:isopropyl alcohol = 1:3) for 60 s to remove the exposed PMMA photoresist and create the reservoirs. The CNT parts in the reservoirs were exposed to air, which were removed by oxygen plasma treatments [Fig. 1(c)]. At the same time, the oxygen plasma treatments also opened the CNT ends to ensure fluid flows. The length of the CNTs involved in the fluidic chip was controlled by

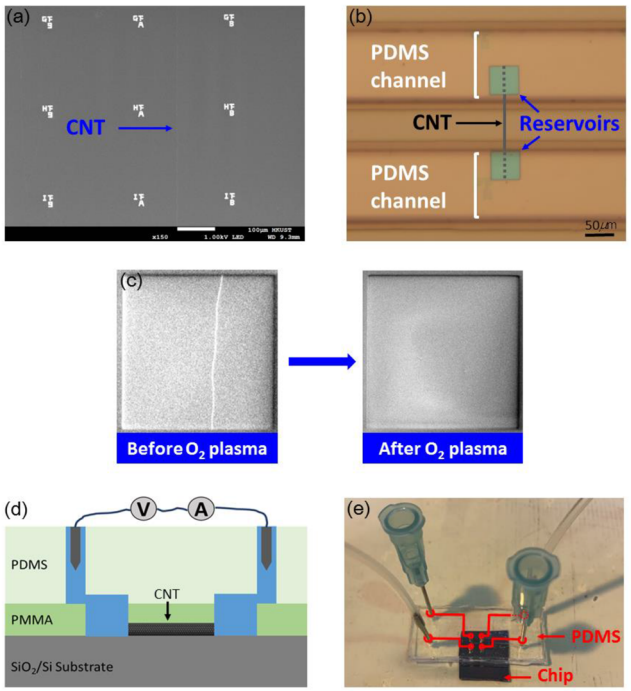

FIG. 1. CNT synthesis and experiment. (a) Scanning electron microscopy (SEM) image of a SWCNT grown on a silicon oxide substrate. (b) Optical microscope image of two patterned reservoirs (green areas) covered by a PDMS microfluidic system. (c) SEM image of a reservoir and the exposed part of CNT before and after O_2 plasma treatment. (d) Schematic of the CNT-based nanofluidic device. (e) An assembled device.

the spacing between the two reservoirs. To prevent potential leakage from PMMA, a typical length of 100 μm was employed. Finally, a polydimethylsiloxane (PDMS) cover embedded with microchannels was bonded onto the PMMA layer, as illustrated in Fig. 1(b). The microchannels in the PDMS cover connect the reservoirs with outer fluidic pathways.

C. Experimental setup

Figure 1(d) depicts the schematic of the nanofluidic device, and Fig. 1(e) shows the picture of an assembled device. In each device, one SWCNT or a few (up to five) are used. The ionic currents generated by the flows of potassium chloride (pH = 6) were measured by using Ag/AgCl electrodes (BASi, MF-2078, 3.0 M NaCl), which were attached to an Axopatch 200B amplifier (Molecular Devices, Sunnyvale, CA) in the voltage-clamp configuration. All the measurements were performed in a Faraday cage.

D. CNT diameter measurement

Atomic force microscopy (AFM) was employed to determine the diameters of SWCNTs in the tapping-mode. Figure S1(a) shows an AFM image for CNT characterization. The CNT diameter distribution is depicted in Fig. S1(b), which fell in the range of 0.8 nm –3.2 nm and the median diameter was 1.6 nm.

E. Raman spectroscopy characterization

The resonance Raman data of individual SWCNTs were collected using a confocal imaging microscope combined with micro-Raman spectroscopy at an excitation wavelength of 532 nm (the excitation spot size was about 1 μm in diameter). The G-band of Raman spectra revealed that the CNTs were semiconducting or metallic CNTs.[39] Representative spectra for semiconducting and metallic CNTs are shown in Figs. S2(a) and S2(b).

F. Control experiments and experimental details

To confirm that the currents were caused by the transport of ions instead of the electric leakage, control experiments were also performed, where devices without CNTs were fabricated through the same process as that for the CNT-based fluidic systems. Figure S3 shows the currents of three control devices as a function of the ion concentration. It is seen that the currents are roughly independent of the ion concentration and remain low (below 3 pA), which is considered as the background current. The results in Fig. S3 also indicate that O_2 plasma treatment did not cause significant current leakage. Totally 80 devices were fabricated; however, only about 10% of them worked, where measurable ionic currents were found. Such a low yielding rate might be caused by the CNT entrance blockage due to contaminations or certain defects in CNTs.

G. MD Simulation

Non-equilibrium MD simulations are performed using the Large-scale Atomic/Molecular Massively Parallel Simulator (LAMMPS) package.[40–43] The dimension of the simulation box is $7.4 \times 7.7 \times 17.5\,\text{nm}^3$, with periodic boundary conditions applied in all the three directions. The simulation system contains a 9.8-nm-long (10, 10) CNT (1.36 nm in diameter) with/without functional groups (COO^-) at the ends. The CNT is connected to two reservoirs filled with water molecules and ions, as shown in Fig. 2. COO^- molecules are described by the all-atom optimized potentials for liquid simulations (OPLS-AA) force field[44] and water molecules are simulated with the extended simple point-charge

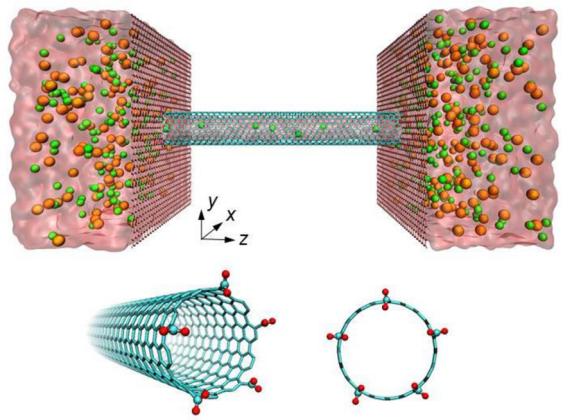

FIG. 2. Molecular dynamics simulation system: A CNT with two reservoirs at the ends. Green, orange, red, and cyan spheres are potassium ions, chloride ions, oxygen atoms of COO^-, and carbon atoms of COO^-, respectively. Water molecules are shown as transparent cloud.

(SPC/E) water model.[45] Potassium and chloride ions are modeled by the Lennard-Jones and Coulombic potentials, and the parameters are adopted from Ref. 46. By introducing a uniform partial charge, $-0.005e$, to each carbon atom, the surface charge density of the CNT is set as $-0.03\,\mathrm{C/m^2}$, which is within the range of practical cases.[23] To verify the role of functional groups, cases of 0, 5, and 10 carboxylate groups at each end of the CNT are studied. These numbers of carboxylate groups could be experimentally achieved by considering various factors, such as the chemical sites, electrical repulsion, and rim deformation.[47] Electroneutrality is ensured for all the cases by adding additional cations to the system to balance the carboxylate groups and the surface charges of the CNT. During the simulations, all the wall atoms are fixed except the COO^- groups. The bond length and angle of water molecules are constrained by the SHAKE algorithm. The long-range Coulombic interactions are accounted for with the Particle–Particle Particle–Mesh (PPPM) method. The temperature of the system is maintained at 300 K by applying a Nóse–Hoover thermostat to the degrees of freedom of water molecules and ions in the x and y directions (perpendicular to the axial direction of the CNT). The time step is set at 1.0 fs.

In the simulations, the electric field is applied in the z direction (axial direction of the CNT) with the magnitude in the range of

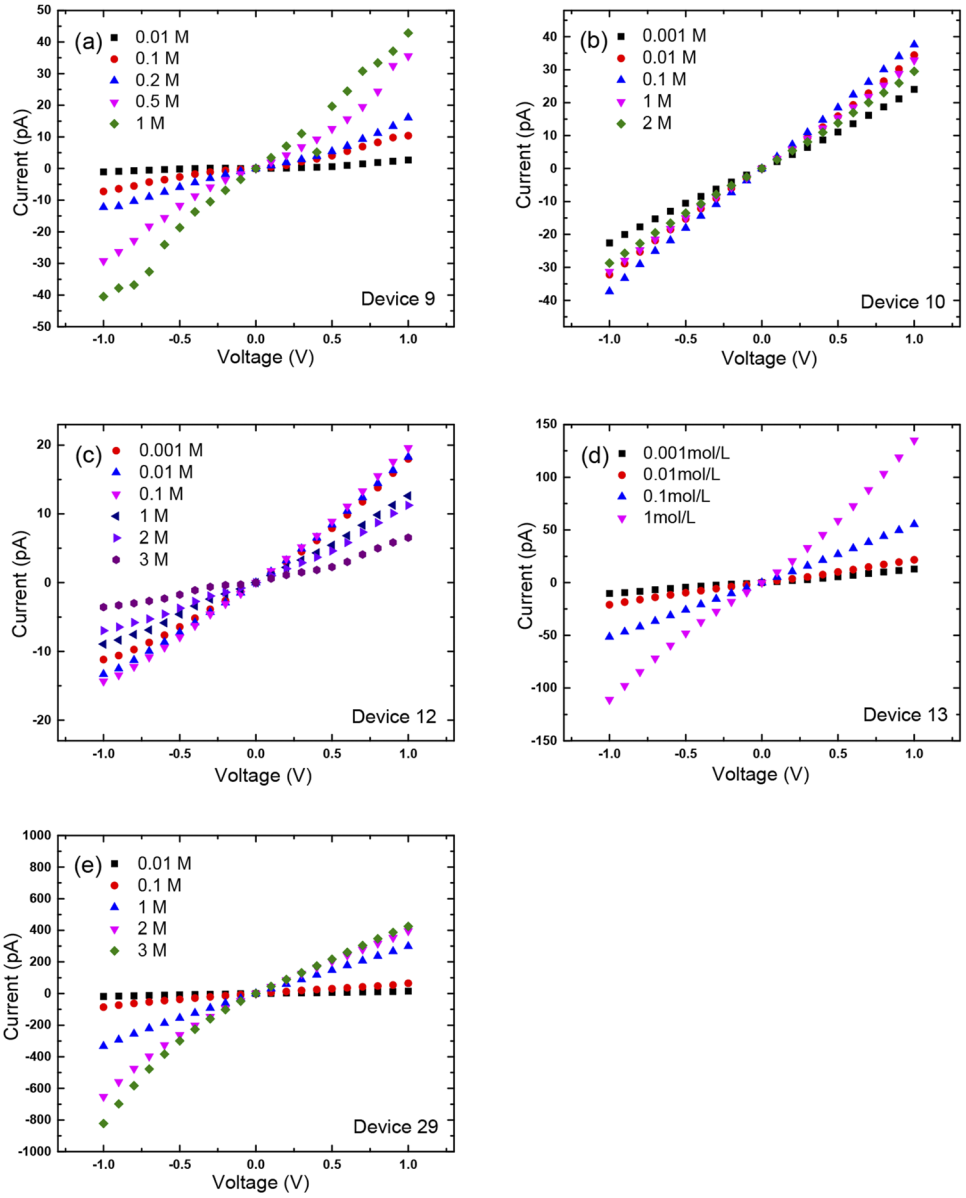

FIG. 3. *I–V* characteristics at various concentrations for different devices. (a) Device 9. (b) Device 10. (c) Device 12. (d) Device 13. (e) Device 29.

0 V/Å–0.015 V/Å. The simulation system is relaxed for 5 ns first to reach the steady state. The following 35 ns is used for data collection. The ionic current is calculated as $I = N_t/\Delta t$, where N_t is the number of ions entering the CNT within a time interval Δt, which is set as 2.5 ns. Conductance G is obtained as $G = I/V$. 14 simulations with different initial conditions are carried out to obtain the average current and the error bar for each case.

To consider the free energy profile of individual ions (cations) in the CNT, the potential of mean force (PMF) is obtained by using umbrella sampling and Weighted Histogram Analysis Method (WHAM).[48] A 2 nm long path across the CNT entrance is split into 20 windows of equal width (1 Å) in the z direction. An ion is constrained in each region by a harmonic spring in the axial direction, with the spring constant equal to 2.0 kcal/(mol·Å^2). Each configuration is first equilibrated for 5 ns, after which the simulation is performed for 15 ns to calculate the PMF. The energy barrier ΔE is calculated as the difference between the maximum and minimum values of the PMF.

The residence time of cations at the CNT entrance is computed to capture the interaction between ions and functional groups at the CNT entrance. The residence time is calculated as the average time of each migrating cation dwelling at the entrance region, which is defined as a cylindrical region between $z = -4$ Å and $z = 4$ Å with the radius equal to 8 Å (the entrance is at $z = 0$).

III. RESULTS AND DISCUSSION

By applying external voltages, I–V curves at different ion concentrations for various devices were obtained, as shown in Figs. 3(a)–3(e) [the distribution of CNT diameters can be found in Fig. S1(b)]. Generally, three distinct I–V curves were observed: linear, nonlinear, and asymmetric relationships. However, these I–V behaviors depend on the device and are affected by the ion concentration {e.g., linear dependence is found at low ion concentrations in device 13 [Fig. 3(d)], while it tends to occur at high concentrations in device 9 [Fig. 3(a)]}. Asymmetric I–V relationships were found in devices 12, 13, and 29, as the ion concentrations were varied. To clearly present the results by considering the effect of ion concentration, the ionic conductance G, which is defined $G = I/V$ (for nonlinear and asymmetric I–V curves, G is obtained at $V = 1$ V), as a function of ion concentration C is illustrated, as depicted in Fig. 4 for different devices. Figure 4(a) shows G for devices 9, 13, and 29. It is seen that the relationship between G and C follows the power-law dependence, i.e., $G \propto C^{\alpha}$, which is consistent with most previous experiments.[19–25] However, the power α assumes different values, ranging from 0.36 to 0.72, for different devices and its value slightly depends on the ion transport direction. This is different from previous studies, where a constant α was found for all the devices. If the normalized conductance, $G^* = G/G_o$, where G_o is the conductance at $C = 1$ M, is considered, the $G^* - C$ data for devices 9 and 29 roughly fall onto the same line in logarithmic coordinates because they share similar α, as shown in the inset of Fig. 4(a).

For devices 10 and 12, however, G increases first and then decreases with the increase in C, as shown in Fig. 4(b), which is completely different from the results in Fig. 4(a). Such behavior has been barely observed. It is interesting that such a G–C dependence is similar to some biological nanochannels,[49–51] as indicated by the olive diamond symbols in Fig. 4(b), which are the results for a gramicidin A (gA) biological nanochannel embedded in a negatively charged membrane.[49]

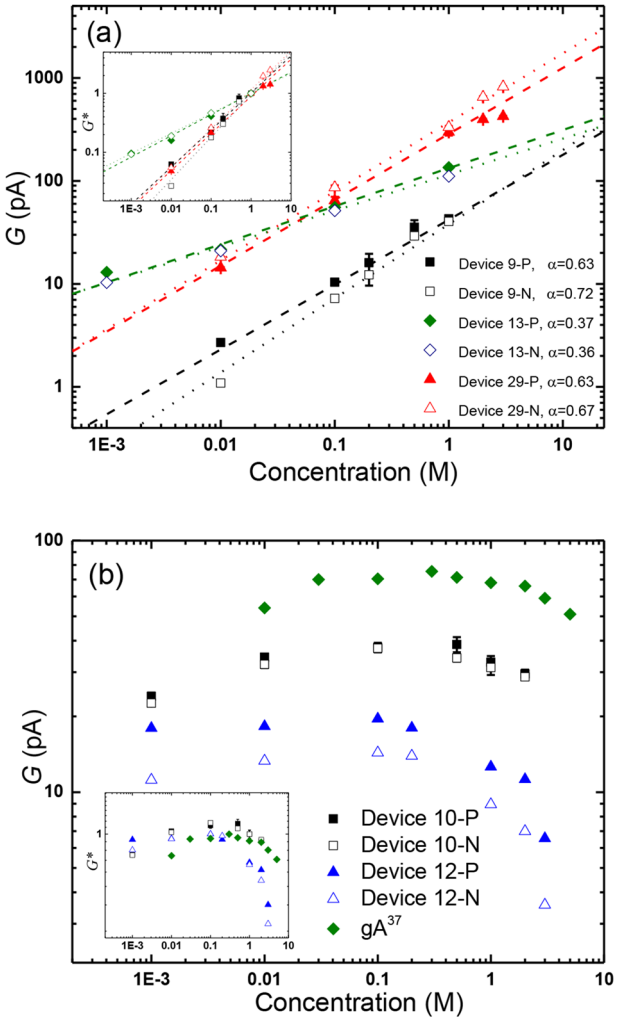

FIG. 4. Ionic conductance as a function of ion concentration. "P" and "N" denote that the current is obtained under a positive and a negative voltage, respectively. (a) G–C relations showing power-law dependences (dashed and dotted lines are power-law fits of the data). (b) Non-power-law G–C relationship. The insets in (a) and (b) show the normalized conductance G^*.

In the literature, the power-law dependence of G on C [Fig. 4(a)] was explained as a consequence of surface functionalization[21] in thick CNTs or electro-osmotic flows[19,23] and strong water–ion interactions[24] in thin CNTs. In addition to power-law G–C relationships, previous work found increasing and then saturated G with the increase in C and the saturation was attributed to ion–ion interactions, which set a limit for the ion concentration in the CNT.[22] These explanations might have caught the underlying physics for certain specific cases. However, they cannot elucidate all the conductance behavior in Fig. 4, especially the decrease in G at high ion concentrations in Fig. 4(b). A recent theoretical study attributes various power-law relationships in nanopores to the

charge imbalance between the pore surface and the solution inside the pore.[52] The theory works well for certain nanoconfinements but fails in explaining the ion transport in CNTs. This indicates that rather than surface charges, there should be other dominant factors for CNTs.

As the CNT diameters in this work were small, the entrance properties should play an important role in affecting the ion transport, as reported in previous studies on ion transport in CNTs and graphene oxide nanopores.[53,54] In fabricating the fluidic chips, the CNTs were opened by oxygen-plasma treatments, which could have functionalized the CNT ends with COO^- groups.[35] The COO^- groups can change the potential distribution and the energy barrier at the entrance, which are fundamental factors governing the ion transport at the nanoscale. Unfortunately, it is difficult to determine the number of COO^- groups at the CNT ends experimentally. To probe the role of COO^- groups, non-equilibrium MD simulations are performed. In the simulations, the ionic currents are calculated by changing the number of COO^- groups, N_{COO^-}, at the CNTs ends [the migration ions in a CNT are shown in Fig. 5 (Multimedia view)]. The $G - C$ dependence for different N_{COO^-} values is shown in Fig. 6(a). When the CNT ends are free of COO^- groups ($N_{COO^-} = 0$), G increases linearly with the increase in C. Once there are COO^- groups, the linear G–C relationship does not hold. At $N_{COO^-} = 5$, a power-law dependence, $G \propto C^{\alpha}$ with $\alpha = 0.52$, is found for $C < 1$ M, as shown in Fig. 6(a). This is generally in good agreement with the experimental results for devices 9 and 29 [see Fig. 4(a)]. For $N_{COO^-} = 10$, the $G - C$ behavior becomes similar to the experimental results in Fig. 4(b), where G increases and then decreases when C is increased.

The MD results confirm the importance of entrance functionalization. As discussed previously, the functional groups at the CNT ends vary the potential distribution at the entrance and affect the ion transport. Therefore, the PMF for ions at the CNT entrance is calculated. Figure 7 shows the PMF around the CNT entrance for the cases of $N_{COO^-} = 0$ and 5. It is clear that there is an energy barrier ΔE, which is the PMF difference between the minimum and maximum near the entrance, for all the cases. The probability P of an ion overcoming this energy barrier is determined by the kinetic energy of the ion and the energy barrier, i.e., $P \propto \exp(-\Delta E/k_B T)$, where k_B is the Boltzmann constant and T is the temperature. Hence, a large ΔE hinders the transport of ions. In Fig. 7, it is seen that ΔE is roughly independent of the concentration if the CNT entrance is free of functional groups [$N_{COO^-} = 0$; Fig. 7(a)], while it increases

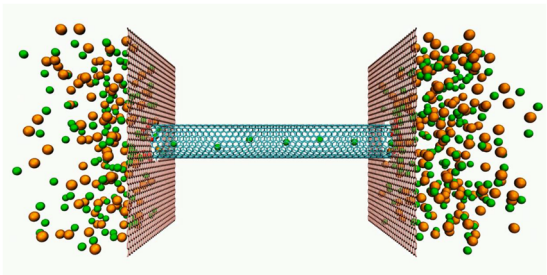

FIG. 5. Ion migration in a CNT ($N_{COO^-} = 5$ at $C = 1$ M). Multimedia view: https://doi.org/10.1063/5.0037208.1

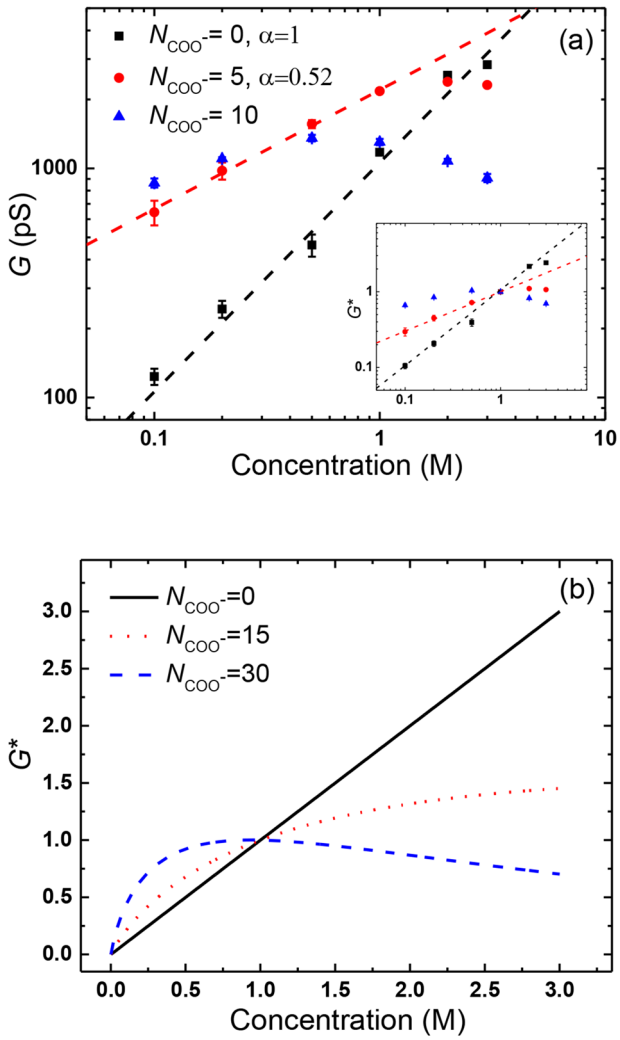

FIG. 6. Ionic conductance as a function of electrolyte concentration with different N_{COO^-} obtained by (a) MD simulations (the dashed lines are power-law fits of the data with α given in the legend) and (b) theoretical analysis.

with the increase in the concentration for $N_{COO^-} = 5$ [see Fig. 7(b)]. This indicates that the variation of concentration does not alter the energy barrier when the CNT entrance is unfunctionalized. In this case, the current is mainly determined by the ion concentration and G increases linearly with the increase in C, as shown in Fig. 6(a). For $N_{COO^-} = 5$, however, as C is increased, the increasing ΔE introduces extra resistance and tends to impede the transport of ions, leading to a sub-linear G–C relationship, i.e., power-law dependence, $G \propto C^{\alpha}$ with $\alpha < 1$.

In Fig. 7, it is also shown that ΔE is around 2.3 kcal/mol for unfunctionalized cases. For $N_{COO^-} = 5$, ΔE varies from 1.3 kcal/mol to 2.5 kcal/mol when the ion concentration is increased from 0.1 M to 3 M. This suggests that the functional groups at the CNT entrance can enhance ion transport at low concentrations, while it weakens the ionic current at high concentrations, indicating an

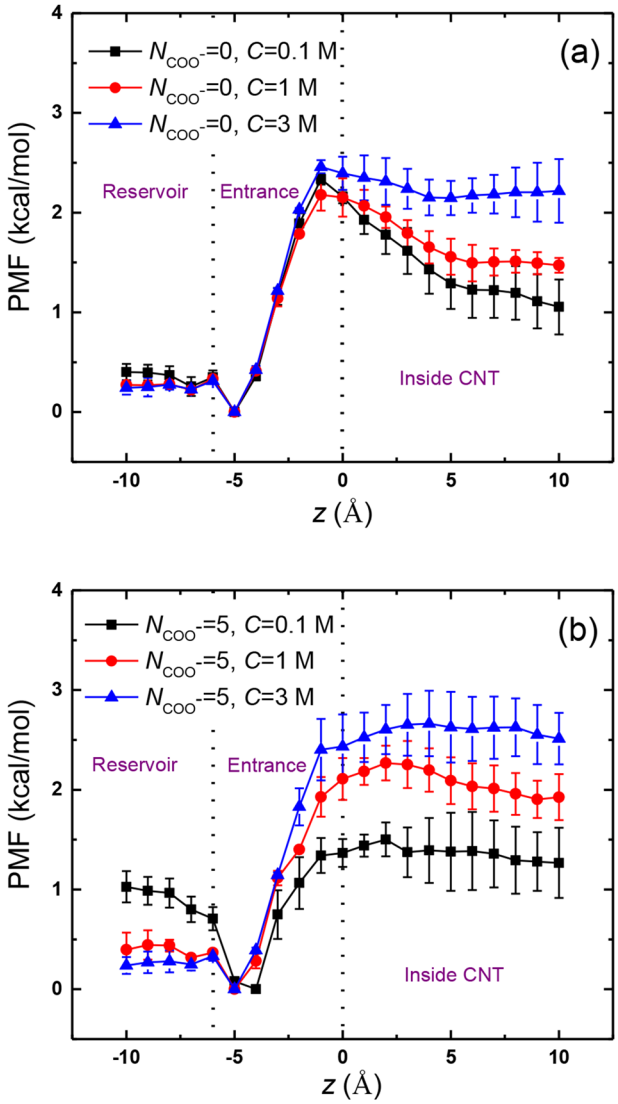

FIG. 7. PMF near the CNT entrance along the axial direction with (a) N_{COO^-} = 0 and (b) N_{COO^-} = 5. Dashed lines indicate the location of reservoir and CNT entrance.

interplay between ion concentration and the functional groups. At low concentrations, COO^- groups attract cations in the reservoir and increases the ion concentration at the entrance region, which, consequently, enhances the ionic current.[22] Although some cations may be dangling briefly at the entrance, they are easily driven into the CNT, as supported by the residence time at low concentrations in Figs. 8 and 9 (Multimedia view). The enhancement caused by COO^- is consistent with previous studies for CNTs and graphene oxide nanopores.[53,54] At high concentrations, however, some cations can be very close to and trapped by the COO^- groups provisionally (see the inset of Fig. 8). This may cause short-time blockages at the CNT entrance, leading to high energy barriers [Fig. 7(b)], as indicated by the long residence time at high concentrations in

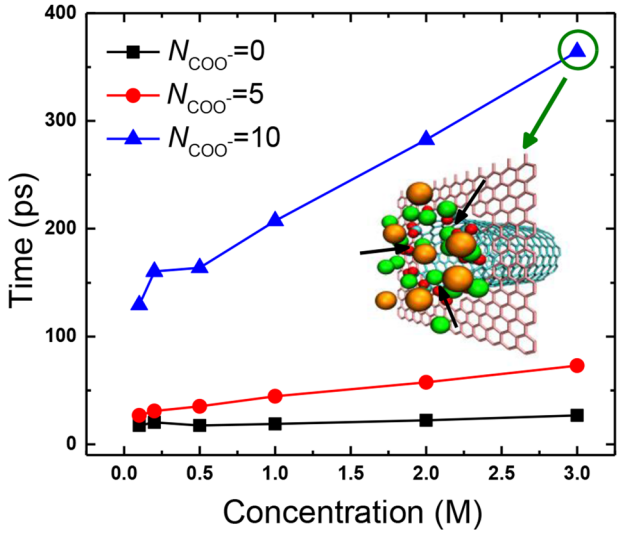

FIG. 8. Residence time for cations at the entrance region of the CNT. The inset shows a snapshot of K^+ trapped by the COO^- groups (see Fig. 4) provisionally. The black arrows indicate the K^+ (green) trapped by the COO^- groups.

Figs. 8 and 10 (Multimedia view). Furthermore, Fig. 8 also illustrates that the residence time strongly depends on N_{COO^-} [also see Figs. 10–12 (Multimedia views)], which indicates that the heavily functionalized CNT is quite sensitive to the variation of the ion concentration.

It is worth mentioning that the valley in PMF next to the entrance of the CNT in Fig. 7 is mainly caused by the electrostatic attraction due to the COO^- groups at the CNT entrance. For unfunctionalized CNTs, it remains largely unchanged [Fig. 7(a)]. In the presence of COO^- groups, the attraction is enhanced at low ion concentrations, for which the valley becomes clearer. At high ion concentrations, however, the COO^- groups tend to be neutralized

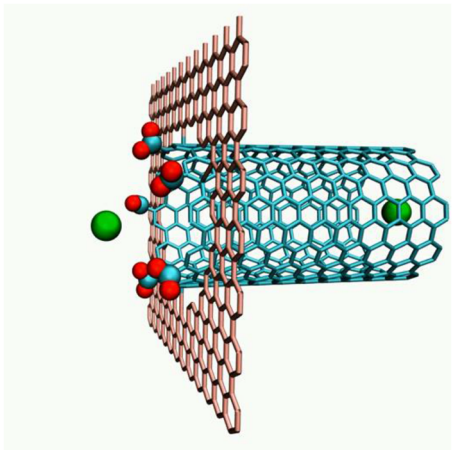

FIG. 9. Motion of ions at the entrance region (N_{COO^-} = 5 at C = 0.1 M). Multimedia view: https://doi.org/10.1063/5.0037208.2.

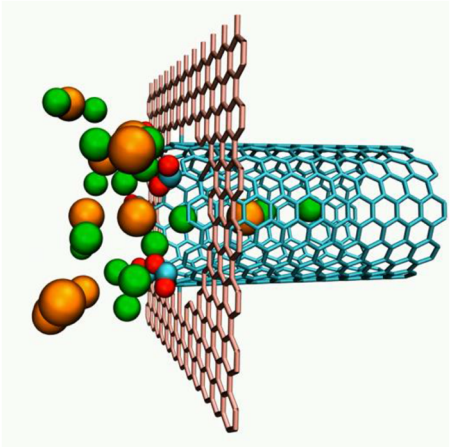

FIG. 10. Motion of ions at the entrance region (N_{COO^-} = 5 at C = 3 M). Multimedia view: https://doi.org/10.1063/5.0037208.3

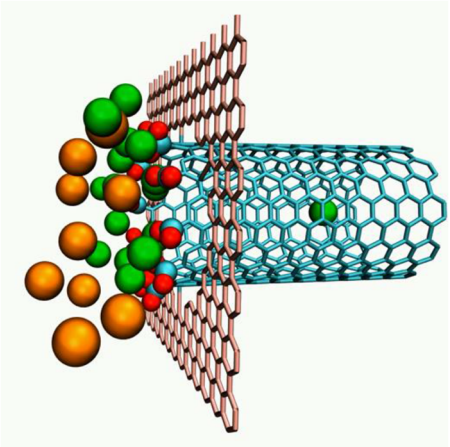

FIG. 12. Motion of ions at the entrance region (N_{COO^-} = 10 at C = 3 M). Multimedia view: https://doi.org/10.1063/5.0037208.5

by K^+, which weakens the attraction and consequently the shape of the PMF valley. Furthermore, the entrance functionalization is expected to be critical for small-diameter CNTs (e.g., $d < 2$ nm), where it greatly affects the value of α for the G–C relation. For large-diameter CNTs, the G–C relationship should tend to be linear as the CNT diameter is increased and the value of α will converge to unity.

With the above fundamental information about the roles of entrance functionalization and its interplay with ion concentration, it is ready to explain the experimental results in Fig. 4. First of all, all the CNTs in the devices in Fig. 4 were functionalized because linear G–C relationships were not observed. Second, the number of functional groups at the CNT entrances varied for different devices. In devices 9 and 29, which had similar α values (0.63–0.72), the number of COO^- groups was relatively small. In device 9, the number of COO^- groups should be higher than devices 9 and 29, as suggested by a smaller α value (~0.36). For devices 10 and 12 in Fig. 4(b), however, heavy functionalization of CNT entrances was implied because the conductance decreases at high concentrations, which is consistent with N_{COO^-} = 10 in Fig. 6(a). These explanations also clarify the inconsistency in previous studies.[19–25]

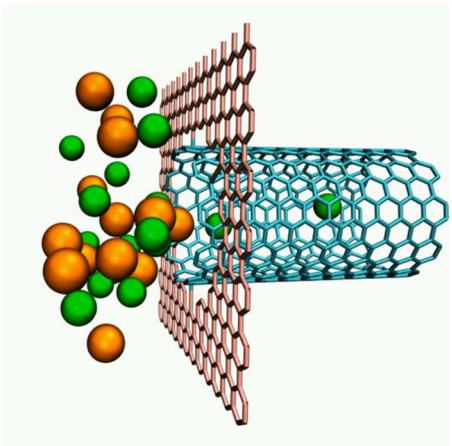

FIG. 11. Motion of ions at the entrance region (N_{COO^-} = 0 at C = 3 M). Multimedia view: https://doi.org/10.1063/5.0037208.4

The G–C relationships in Fig. 4 can also be described using the electrokinetic theory by considering the entrance functionalization. A CNT can be modeled as a cylindrical tube with radius r and length L. As the CNT diameter is small and the surface is negatively charged, it is reasonable to assume that only cations transport through the CNT. The total potential for the cations, ϕ, includes the potential generated by the external electric field, ϕ_E, and that due to the internal charges, i.e., the surface and entrance charges, ϕ_S and ϕ_{COO^-}, respectively. Thus, ϕ is written as

$$\phi = \phi_E + \phi_S + \phi_{COO^-}. \tag{1}$$

For long tubes, the potential distribution induced by the surface charges is approximated as[55]

$$\phi_S = \begin{cases} 2\tilde{z}\phi_S(\tilde{z}=0.5) & 0 \le \tilde{z} \le 0.5, \\ -2(\tilde{z}-1)\phi_S(\tilde{z}=0.5) & 0.5 < \tilde{z} \le 1, \end{cases} \tag{2}$$

where $\tilde{z} = z/L$. The peak value $\phi_S(\tilde{z}=0.5)$ depends on the surface charge density σ. Equation (2) has been found working well for infinitely long tubes.[56] For small-diameter tubes, the entrance functional groups play a dominant role in affecting the ion transport compared with the surface charges. According to the Gouy–Chapman theory,[22,57] the electrostatic potential induced by COO^- groups at the entrance can be estimated as

$$\phi_{COO^-} = \frac{eN_{COO^-}}{4\pi\varepsilon_0\varepsilon r} e^{-r/\lambda_D}, \tag{3}$$

where ε_0 and ε are the absolute dielectric constant of vacuum and the relative dielectric constant of water, respectively, and $\lambda_D = \sqrt{\varepsilon\varepsilon_0 RT/(2F^2C)}$ is the Debye length (herein, R and F are the gas

constant and Faraday constant, respectively). The flux of ions, J, satisfies the one-dimensional Nernst–Planck equation,[58,59]

$$-\frac{d}{dz}J(z) = \frac{d}{dz}D\left(\frac{dC}{dz} + C\frac{e}{k_B T}\frac{d\phi}{dz}\right) = 0, \tag{4}$$

where D is the diffusion coefficient of ions. If the dimensionless coordinate $\tilde{z} = z/L$ is used, J is given by

$$J = D\frac{C(0)e^{e\phi(0)/k_B T} - C(1)e^{e\phi(1)/k_B T}}{\int_0^1 e^{e\phi(\tilde{z})/k_B T}d\tilde{z}}, \tag{5}$$

where $C(0)$ and $C(1)$ are the concentrations at the inlet and outlet of the CNT. If $C(0) = C(1) = C_{\text{bulk}}$ is employed,[59] the electric current is obtained as[55]

$$I = F\pi r^2 J/L. \tag{6}$$

The conductance G is then calculated as $G = I/\phi_E$. As N_{COO^-} affects the conductance, the normalized conductance $G^* = G/G_o$ is computed, where G_o is the conductance at $C = 1$ M. The dependence of G^* on C is shown in Fig. 6(b). A linear relationship is found for the unfunctionalized case ($N_{COO^-} = 0$), which agrees well with MD simulations [Fig. 6(a)]. For $N_{COO^-} = 15$, the $G^* - C$ dependence follows a power law. At $N_{COO^-} = 30$, G^* increases first and then drops as C is increased. The $G^* - C$ relationships with entrance functionalization in Fig. 6(b) are consistent with experiments shown in Fig. 4 and confirm the roles of COO^- groups discussed previously.

The distinct effects of CNT entrance functionalization on the ionic conductance may be utilized to achieve various tasks in practical applications.[14,22,35] However, the number of functional groups, N_{COO^-}, at the entrance is uncontrollable. During the fabrication of the fluidic system, the time of plasma treatment for opening CNT ends varies for different devices. This is because the CNT diameters in various devices are different. Another reason lies in the structure of CNT, such as CNT's chirality. Furthermore, the interaction between the CNT and the substrate (e.g., the adhesive force), which is caused by the CNT growth environment, also affects the time of plasma treatment. In addition to the plasma treatment and chemical and electrostatic doping caused by the surrounding materials, humidity and fluid/solution properties also affect the functionalization at the CNT entrance. All these factors make the functionalization an uncertain process and the number of functional groups at the CNT entrance becomes uncontrollable. This is why different experiments show different G–C relationships in previous work. The uncertainty in G–C dependence imposes a challenge to the applications of CNT-based nanofluidic devices. Therefore, sophisticated experimental techniques for precisely controlling the entrance functionalization of CNT are desired for practical applications.

IV. CONCLUSIONS

In summary, we have conducted experiments, MD simulations, and theoretical analysis to study ion transport in CNTs. Diverse G–C relationships have been observed, which are determined by the COO^- groups at the CNT entrances. The intrinsic uncontrollability of the number of COO^- groups imposes a challenge to the practical applications of CNT-based nanofluidic systems.

SUPPLEMENTARY MATERIAL

See the supplementary material for device characterization and experimental data from control devices.

AUTHORS' CONTRIBUTIONS

R.T., X.G., and D.L. contributed equally to this work.

ACKNOWLEDGMENTS

This work was supported by the Research Grants Council of the Hong Kong Special Administrative Region under Grant No. 16209119.

The authors declare no conflict of interest.

DATA AVAILABILITY

The data that support the findings of this study are available within the article and its supplementary material.

REFERENCES

[1] R. B. Schoch, J. Han, and P. Renaud, "Transport phenomena in nanofluidics," Rev. Mod. Phys. **80**, 839 (2008).
[2] Z. Cheng, Z. Ning, W. Zhang, and S. Ke, "Theoretical investigation of electroviscous flows in hydrophilic slit nanopores: Effects of ion concentration and pore size," Phys. Fluids **32**, 022005 (2020).
[3] Z. Li, *Nanofluidics: An Introduction* (CRC Press, 2018).
[4] E. Amani, M. Mehrabian, and S. Movahed, "A discrete phase hybrid continuum-atomistic model for electrokinetics in nanofluidics," Phys. Fluids **30**, 072003 (2018).
[5] X. Gao, T. Zhao, and Z. Li, "Controlling flow direction in nanochannels by electric field strength," Phys. Rev. E **92**, 023017 (2015).
[6] C.-C. Chang, R.-J. Yang, M. Wang, J.-J. Miau, and V. Lebiga, "Liquid flow retardation in nanospaces due to electroviscosity: Electrical double layer overlap, hydrodynamic slippage, and ambient atmospheric CO_2 dissolution," Phys. Fluids **24**, 072001 (2012).
[7] Y. Jin, R. Tao, and Z. Li, "Understanding flow enhancement in graphene-coated nanochannels," Electrophoresis **40**, 859 (2019).
[8] S. Luo, C. Li, F. Li, J. Wang, and Z. Li, "Ice crystallization in shear flows," J. Phys. Chem. C **123**, 21042 (2019).
[9] S. Ghosh, A. Sood, and N. Kumar, "Carbon nanotube flow sensors," Science **299**, 1042 (2003).
[10] J. Wu, K. S. Paudel, C. Strasinger, D. Hammell, A. L. Stinchcomb, and B. J. Hinds, "Programmable transdermal drug delivery of nicotine using carbon nanotube membranes," Proc. Natl. Acad. Sci. U. S. A. **107**, 11698 (2010).
[11] H. G. Park and Y. Jung, "Carbon nanofluidics of rapid water transport for energy applications," Chem. Soc. Rev. **43**, 565 (2014).
[12] F. Faraji and A. Rajabpour, "Temperature gradient-induced fluid pumping inside a single-wall carbon nanotube: A non-equilibrium molecular dynamics study," Phys. Fluids **28**, 092004 (2016).
[13] A. Kalra, S. Garde, and G. Hummer, "Osmotic water transport through carbon nanotube membranes," Proc. Natl. Acad. Sci. U. S. A. **100**, 10175 (2003).
[14] B. Corry, "Water and ion transport through functionalised carbon nanotubes: Implications for desalination technology," Energy Environ. Sci. **4**, 751 (2011).
[15] F. Fornasiero, H. G. Park, J. K. Holt, M. Stadermann, C. P. Grigoropoulos, A. Noy, and O. Bakajin, "Ion exclusion by sub-2-nm carbon nanotube pores," Proc. Natl. Acad. Sci. U. S. A. **105**, 17250 (2008).
[16] H. Sui, B.-G. Han, J. K. Lee, P. Walian, and B. K. Jap, "Structural basis of water-specific transport through the AQP1 water channel," Nature **414**, 872 (2001).

[17]T. I. Brelidze, X. Niu, and K. L. Magleby, "A ring of eight conserved negatively charged amino acids doubles the conductance of BK channels and prevents inward rectification," Proc. Natl. Acad. Sci. U. S. A. **100**, 9017 (2003).
[18]S. Dalla Bernardina, E. Paineau, J.-B. Brubach, P. Judeinstein, S. Rouzière, P. Launois, and P. Roy, "Water in carbon nanotubes: The peculiar hydrogen bond network revealed by infrared spectroscopy," J. Am. Chem. Soc. **138**, 10437 (2016).
[19]H. Liu, J. He, J. Tang, H. Liu, P. Pang, D. Cao, P. Krstic, S. Joseph, S. Lindsay, and C. Nuckolls, "Translocation of single-stranded DNA through single-walled carbon nanotubes," Science **327**, 64 (2010).
[20]S. Guo, S. F. Buchsbaum, E. R. Meshot, M. W. Davenport, Z. Siwy, and F. Fornasiero, "Giant conductance and anomalous concentration dependence in sub-5 nm carbon nanotube nanochannels," Biophys. J. **108**, 175a (2015).
[21]E. Secchi, A. Niguès, L. Jubin, A. Siria, and L. Bocquet, "Scaling behavior for ionic transport and its fluctuations in individual carbon nanotubes," Phys. Rev. Lett. **116**, 154501 (2016).
[22]H. Amiri, K. L. Shepard, C. Nuckolls, and R. Hernández Sánchez, "Single-walled carbon nanotubes: Mimics of biological ion channels," Nano Lett. **17**, 1204 (2017).
[23]P. Pang, J. He, J. H. Park, P. S. Krstić, and S. Lindsay, "Origin of giant ionic currents in carbon nanotube channels," ACS Nano **5**, 7277 (2011).
[24]Y.-C. Yao, A. Taqieddin, M. A. Alibakhshi, M. Wanunu, N. R. Aluru, and A. Noy, "Strong electroosmotic coupling dominates ion conductance of 1.5 nm diameter carbon nanotube porins," ACS Nano **13**, 12851 (2019).
[25]R. H. Tunuguntla, R. Y. Henley, Y.-C. Yao, T. A. Pham, M. Wanunu, and A. Noy, "Enhanced water permeability and tunable ion selectivity in subnanometer carbon nanotube porins," Science **357**, 792 (2017).
[26]J. Wu, K. Gerstandt, H. Zhang, J. Liu, and B. J. Hinds, "Electrophoretically induced aqueous flow through single-walled carbon nanotube membranes," Nat. Nanotechnol. **7**, 133 (2012).
[27]K. Yazda, S. Tahir, T. Michel, B. Loubet, M. Manghi, J. Bentin, F. Picaud, J. Palmeri, F. Henn, and V. Jourdain, "Voltage-activated transport of ions through single-walled carbon nanotubes," Nanoscale **9**, 11976 (2017).
[28]J. Geng, K. Kim, J. Zhang, A. Escalada, R. Tunuguntla, L. R. Comolli, F. I. Allen, A. V. Shnyrova, K. R. Cho, D. Munoz, Y. M. Wang, C. P. Grigoropoulos, C. M. Ajo-Franklin, V. A. Frolov, and A. Noy, "Stochastic transport through carbon nanotubes in lipid bilayers and live cell membranes," Nature **514**, 612 (2014).
[29]X. Gao, T. Zhao, and Z. Li, "Fluid breakup in carbon nanotubes: An explanation of ultrafast ion transport," Phys. Fluids **29**, 092003 (2017).
[30]P. Biesheuvel and M. Bazant, "Analysis of ionic conductance of carbon nanotubes," Phys. Rev. E **94**, 050601 (2016).
[31]J. A. Thomas and A. J. McGaughey, "Water flow in carbon nanotubes: Transition to subcontinuum transport," Phys. Rev. Lett. **102**, 184502 (2009).
[32]J. A. Thomas and A. J. H. McGaughey, "Density, distribution, and orientation of water molecules inside and outside carbon nanotubes," J. Chem. Phys. **128**, 084715 (2008).
[33]A. I. Kolesnikov, J.-M. Zanotti, C.-K. Loong, P. Thiyagarajan, A. P. Moravsky, R. O. Loutfy, and C. J. Burnham, "Anomalously soft dynamics of water in a nanotube: A revelation of nanoscale confinement," Phys. Rev. Lett. **93**, 035503 (2004).
[34]J. Mo, L. Li, J. Zhou, D. Xu, B. Huang, and Z. Li, "Fluid infiltration pressure for hydrophobic nanochannels," Phys. Rev. E **91**, 033022 (2015).
[35]S. S. Wong, E. Joselevich, A. T. Woolley, C. L. Cheung, and C. M. Lieber, "Covalently functionalized nanotubes as nanometre- sized probes in chemistry and biology," Nature **394**, 52 (1998).
[36]X. Zhang, W. Zhou, F. Xu, M. Wei, and Y. Wang, "Resistance of water transport in carbon nanotube membranes," Nanoscale **10**, 13242 (2018).
[37]Y. Li, W. Kim, Y. Zhang, M. Rolandi, D. Wang, and H. Dai, "Growth of single-walled carbon nanotubes from discrete catalytic nanoparticles of various sizes," J. Phys. Chem. B **105**, 11424 (2001).
[38]D. Lin, S. Zhang, W. Liu, Y. Yu, and J. Zhang, "Carburization of Fe/Ni catalyst for efficient growth of single-walled carbon nanotubes," Small **15**, 1902240 (2019).
[39]A. Jorio, A. Souza Filho, G. Dresselhaus, M. Dresselhaus, A. Swan, M. Ünlü, B. Goldberg, M. Pimenta, J. Hafner, and C. Lieber, "G-band resonant Raman study of 62 isolated single-wall carbon nanotubes," Phys. Rev. B **65**, 155412 (2002).
[40]S. Plimpton, "Fast parallel algorithms for short-range molecular dynamics," J. Comput. Phys. **117**, 1 (1995).
[41]S. Luo, J. Wang, and Z. Li, "Homogeneous ice nucleation under shear," J. Phys. Chem. B **124**, 3701–3708 (2020).
[42]B. V. Raghavan and M. Ostoja-Starzewski, "Shear-thinning of molecular fluids in Couette flow," Phys. Fluids **29**, 023103 (2017).
[43]Y. Jin, T. Ng, R. Tao, S. Luo, Y. Su, and Z. Li, "Coupling effects in electromechanical ion transport in graphene nanochannels," Phys. Rev. E **102**, 033112 (2020).
[44]W. L. Jorgensen, D. S. Maxwell, and J. Tirado-Rives, "Development and testing of the OPLS all-atom force field on conformational energetics and properties of organic liquids," J. Am. Chem. Soc. **118**, 11225 (1996).
[45]H. J. C. Berendsen, J. R. Grigera, and T. P. Straatsma, "The missing term in effective pair potentials," J. Phys. Chem. A **91**, 6269 (1987).
[46]I. S. Joung and T. E. Cheatham III, "Determination of alkali and halide monovalent ion parameters for use in explicitly solvated biomolecular simulations," J. Phys. Chem. B **112**, 9020 (2008).
[47]E. Chełmecka, K. Pasterny, T. Kupka, and L. Stobiński, "DFT studies of COOH tip-functionalized zigzag and armchair single wall carbon nanotubes," J. Mol. Model. **18**, 2241 (2012).
[48]A. Grossfield, WHAM: The weighted histogram analysis method, version 2.06, 2012.
[49]T. K. Rostovtseva, V. M. Aguilella, I. Vodyanoy, S. M. Bezrukov, and V. A. Parsegian, "Membrane surface-charge titration probed by gramicidin A channel conductance," Biophys. J. **75**, 1783 (1998).
[50]B. W. Urban, S. B. Hladky, and D. A. Haydon, "Ion movements in gramicidin pores. An example of single-file transport," Biochim. Biophys. Acta Biomembr. **602**, 331 (1980).
[51]E. Neher, J. Sandblom, and G. Eisenman, "Ionic selectivity, saturation, and block in gramicidin A channels," J. Membr. Biol. **40**, 97 (1978).
[52]Y. Noh and N. R. Aluru, "Ion transport in electrically imperfect nanopores," ACS Nano **14**, 10518 (2020).
[53]S. Joseph, R. J. Mashl, E. Jakobsson, and N. R. Aluru, "Electrolytic transport in modified carbon nanotubes," Nano Lett. **3**, 1399 (2003).
[54]C. Fang, Z. Yu, and R. Qiao, "Impact of surface ionization on water transport and salt leakage through graphene oxide membranes," J. Phys. Chem. C **121**, 13412 (2017).
[55]I. Kosińska, "How the asymmetry of internal potential influences the shape of *I–V* characteristic of nanochannels," J. Chem. Phys. **124**, 244707 (2006).
[56]A. Fuliński, I. Kosińska, and Z. Siwy, "On the validity of continuous modelling of ion transport through nanochannels," Europhys. Lett. **67**, 683 (2004).
[57]M. Przybylski, M. O. Glocker, U. Nestel, V. Schnaible, M. Blüggel, K. Diederichs, J. Weckesser, M. Schad, A. Schmid, and W. Welte, "X-ray crystallographic and mass spectrometric structure determination and functional characterization of succinylated porin from *Rhodobacter capsulatus*: Implications for ion selectivity and single-channel conductance," Protein Sci. **5**, 1477 (1996).
[58]B. Nadler, Z. Schuss, U. Hollerbach, and R. Eisenberg, "Saturation of conductance in single ion channels: The blocking effect of the near reaction field," Phys. Rev. E **70**, 051912 (2004).
[59]R. S. Eisenberg, M. M. Kl/osek, and Z. Schuss, "Diffusion as a chemical reaction: Stochastic trajectories between fixed concentrations," J. Chem. Phys. **102**, 1767 (1995).